

MODELLING OF THE DUCTILE TO BRITTLE TRANSITION OF A LOW ALLOY STEEL

S. Carassou \*, S. Renevey \*, B. Marini \*, A. Pineau †

Mechanical tests on compact tensile (CT) specimens were carried out at 0°C in order to investigate the fracture behaviour in the ductile to brittle transition of a low alloy ferritic steel (A 508 Cl 3). At this temperature, the fracture toughness exhibits an important scatter ( $200 < K_j < 500 \text{ MPa}\sqrt{\text{m}}$ ) associated with a large scatter in the stable crack growth behaviour before cleavage ( $0 < \Delta a < 8 \text{ mm}$ )

An original statistical local approach, assuming that cleavage fracture is triggered by the local stress magnification due to the manganese sulphides clusters (MnS) was used in conjunction with finite elements calculations describing stable crack growth (Rousselier model). Assuming a temperature dependence of the parameter related to the local cleavage fracture stress, the model predicts satisfactorily the experimental behaviour in the ductile to brittle transition.

INTRODUCTION

It is well known that the fracture behaviour of low alloy ferritic steels tested in the ductile to brittle transition close to the upper shelf is strongly scattered, in terms of fracture toughness as well as ductile crack growth before cleavage,  $\Delta a$ . The aim of this work is to predict the cleavage probability to failure related to the amount of stable crack growth, or, which is equivalent, to a load parameter as  $K_j$ .

MATERIAL AND EXPERIMENTS

The composition of the material, taken from a PWR nozzle cut-out, is in weight percent : C=0.16, Mn=1.38, Ni=0.70, Mo=0.50, Si=0.24, Cr=0.17, S=0.008, P=0.005. The microstructure is mainly tempered bainitic, and manganese sulfides (MnS) inclusions are present.

\*CEREM/SRMA CEA / Saclay, Saclay 91191 Gif sur Yvette Cedex, France

†Centre des Matériaux, Ecole des Mines, BP 87 91003 Evry Cedex, France, UMR CNRS N° 7633

## ECF 12 - FRACTURE FROM DEFECTS

Fracture toughness experiments were carried out at 0°C on CT 25 specimens with 20% side groove, tested in the TS orientation. These specimens were instrumented to measure both the load-line displacement,  $\delta$ , and stable crack growth before cleavage,  $\Delta a$ . Stable crack growth was measured using a potential drop technique and checked afterwards. These tests were performed using a servohydraulic machine operating under displacement control with a ramp rate of 0.25 mm/mn. ASTM E 813-87 standards were used to calculate J (or  $K_j = \sqrt{J \cdot E / (1 - \nu^2)}$ ) and the effect of the ductile crack growth on J was taken into account. The results are given in table 1.

**TABLE 1 : J parameter (kJ/m<sup>2</sup>), fracture toughness  $K_j$  (MPa√m), ductile crack growth before cleavage  $\Delta a$ (mm), and experimental probability of occurrence at 0°C**

N°	838	345	354	840	356	845	352	841	353	348	351	843	350	355	349
<b>J</b>	167	224	325	417	545	602	636	686	697	724	734	801	860	952	1097
<b><math>K_j</math></b>	191	222	267	303	346	364	374	388	391	399	402	419	435	457	491
<b><math>\Delta a</math></b>	0,07	0,35	0,41	1,17	1,66	2,65	2,15	2,09	2,41	2,99	2,34	4,02	5,16	6,50	7,44
<b>Pr</b>	0,03	0,10	0,17	0,23	0,30	0,37	0,43	0,50	0,57	0,63	0,70	0,77	0,83	0,90	0,97

The results clearly show the very large scatter of both the fracture toughness and stable ductile crack growth before cleavage, characteristic of the fracture behaviour in the transition.

### MODELLING

#### Ductile fracture model used

To describe the stable crack growth, we used the Rousselier model (1), in which the yield function is given by :

$$F = \frac{\sigma_{eq}}{\rho} + D \cdot \sigma_1 \cdot f \cdot \exp\left(\frac{\sigma_m}{\rho \cdot \sigma_1}\right) - R(p) \quad (1)$$

where  $\rho = (1 - f)/(1 - f_0)$  is the relative density of the material,  $f_0$  and  $f$  are the initial and current void volume fraction,  $\sigma_m$  and  $\sigma_{eq}$  are the hydrostatic and the Von Mises stresses respectively, while  $D$  and  $\sigma_1$  are material parameters and  $R(p)$  is the true stress strain curve. In our calculations, this model is slightly modified by introducing a critical void volume fraction  $f_c$  that stands for the void coalescence : when a Gauss point reaches this critical value, it can no longer transmit any stress.

#### Cleavage fracture model used

This model, applied as a post-processor of finite element calculations, has already been successfully used to predict the fracture behaviour of the same steel on notched tensile (NT) specimens in the temperature range from -150°C to -90°C (2). The BEREMIN's methodology (3) is followed : The model is based on the weakest link assumption, but also assumes that in this steel, the MnS clusters are the defects triggering cleavage.

The ductile zones formed inside the MnS clusters are assumed to concentrate stresses and to initiate cleavage on near classical sites like carbides. The ductile damage zones spreading inside the MnS cluster are therefore considered as Griffith cracks that propagate in unstable way under a critical local load,  $\sigma_c$ .

The fracture of an elementary volume,  $V_0$ , containing one MnS cluster is assumed to occur if the size of the defect, i.e. the size of the cluster, becomes critical in regard to the maximum principal stress. The local cleavage fracture stress,  $\sigma_c$ , can be related to the matrix toughness via the cluster sizes and shapes. The knowledge of the statistical distribution of the volume fraction of inclusions allows to calculate the local probability to failure  $p_r$  of  $V_0$  submitted to a maximum principal stress  $\sigma_1$ . For an exponential distribution of the volume fraction, and penny shaped defects, it was shown (2) :

$$p_r(V_0, \sigma_1) = \exp\left[-\left(\frac{\sigma_c}{\sigma_1}\right)^4\right] \quad (2)$$

where  $\sigma_c$  is the mean local cleavage stress needed to break  $V_0$  : It is related to the mean volume fraction of inclusions and to the local matrix toughness. In case of local non-monotonic loading, (local decrease of stresses associated with damage, for example), the local probability to failure  $p_r$  that has to be considered in each element is the maximum value reached during loading ('memory effect').

The global probability to failure of the whole structure  $P_r$  is then calculated using the weakest link theory and assuming statistical independence of the  $V_0$  :

$$P_r(V) = 1 - \exp\left\{-\exp\left[-\left(\frac{\sigma_c}{\sigma_1}\right)^4\right] \frac{dV}{V_0}\right\} \quad (3)$$

where  $V_p$  is a potentially active zone, in which ductile damage inside clusters is assumed to appear and to lead to a Griffith like defect. This zone is defined by the matrix-inclusion decohesion, that occurs when (4):

$$\sigma_I + \alpha \cdot (\sigma_{eq} - \sigma_0) \geq \sigma_d \quad (4)$$

where  $\sigma_0$  and  $\sigma_{eq}$  are the yield and the Von Mises stresses respectively, while  $\alpha$  is a parameter depending of the shape of the particles and  $\sigma_d$  the critical decohesion stress, and were determined respectively 1.6 and 1120 MPa (4).

## RESULTS

### Finite elements calculations

All the simulations were performed using the finite element software CASTEM2000, developed at C.E.A. We performed 2D plane strain and 3D calculations using both a conventional non linear isotropic elastic-plastic model, and the coupled damaging Rousselier model. For all calculations, large displacement and large strains, were assumed. The true stress-strain curve was determined experimentally, and extrapolated by a power law  $\sigma = k \cdot \epsilon^n$ . The initial volume fraction  $f_0$ , and the size of the mesh  $l_c$  used to model the crack growth are related to material characteristics : They were initially determined by image analysis, and then adjusted by comparing the results of FE calculations with experiment. The values of all parameters used are given in table 2. The value of  $l_c$  is very close to the mean spacing between inclusions clusters.

The global behaviour, in terms of load line displacement curves is shown figure 1 : While the non damaging elastoplastic (ELP) simulations can only predict the linear and the beginning of the non linear overall behaviour, the Rousselier (ROUSS) simulations well reproduce the whole experimental curves, both in 2D plane strains or in 3D. The crack growth  $\Delta a$  versus the J parameter curves are also in good agreement with the experiments (figure2).

TABLE 2 : Parameters used for the Finite Elements calculations

Numerically determined parameters				Experimentally determined parameters				
$\sigma_1$ MPa	D	$f_c$	$l_c$ $\mu\text{m}$	$f_0$	$\sigma_0$ MPa	E GPa	k MPa	n
445	2	$5 \cdot 10^{-2}$	420	$5 \cdot 10^{-4}$	495	200	1008	0.14

Post-processor calculations

For all the calculations, the elementary volume  $V_0$  was taken equal to the mean distance between MnS clusters, determined by image analysis :  $(460\mu\text{m})^3$ . We first applied the model to the CT calculations using the values of  $\sigma_c$  determined on NT specimens at -150°C. Despite the whole experimental results are well described for the NT specimens, the use of the same value of  $\sigma_c$  for CT computations at 0°C leads to a very strong underestimation of the probability to failure for a given load : For instance, the K<sub>j</sub> values determined with 3D Rousselier calculations for 10%, 50% and 90% probability to failure were found respectively equal to 120, 180 and 250 MPa $\sqrt{\text{m}}$ , (to be compared with 220, 390, 460 for the experiment, see table 1).

Therefore, we postulated a temperature dependence of the  $\sigma_c$  parameter, which is related to the local cleavage fracture stress. We determined this value by describing the first experimental data points, i.e. those corresponding to cleavage with very little prior ductile propagation. The values of  $\sigma_c$  thus determined are in table 3.

All the calculations lead to a good description of the data points corresponding to low values of K<sub>j</sub>, but only the 3D Rousselier calculation describes the whole experimental scatter (figure 3). Only very slightly different values of the critical cleavage stress are found : The small decrease of the critical cleavage stress between elastoplastic and

## ECF 12 - FRACTURE FROM DEFECTS

Rousselier calculations, generated by the lost of constraint arising with damage, is of same order for CT 3D calculations at 0°C than for NT calculations at -150°C.

**TABLE 3 : Values of  $\sigma_c$ (MPa) used for the post-processor calculations**

Experiment concerned	NT (-150°C)		CTJ 25 (0°C)			
	ELP	ROUSS	ELP		ROUSS	
Hypothesis of FE calculations	2D Axisymmetric		2D	3D	2D	3D
$\sigma_c$ used (MPa)	2460	2430	2850	2800	2750	2750

As shown in (5) for deep cracks in bending, we found that the opening stress ahead the crack tip is very slightly increased by the ductile propagation. The increase of calculated probability in the vicinity of 300MPa√m is then attributed to the onset of the propagation ( $\Delta a > l_c$ ), when the 'memory effect' takes place. Indeed, at equal values of  $K_j$ , the maximum principal stresses are higher for elastoplastic calculations than for the Rousselier calculations. This tends to demonstrate that the memory effect, which is a way to account for the enlargement of the volume where defects are potentially critical, is predominant compared to the increase of local stresses.

### CONCLUSION

The presented model is based on the fact that in our steel, cleavage is triggered by ductile rupture. Assuming a temperature dependence of the critical cleavage stress, the fracture behaviour in the transition regime is well reproduced. Finally, it seems that the load increases the probability of cleavage fracture through ductile stable crack propagation, producing an increase of critical tested volume, rather than by increase of local stresses.

### REFERENCES

- (1) Rousselier G. "Les modèles de rupture ductile et leurs possibilités actuelles dans le cadre de l'approche locale de la rupture", International seminar on local approach of fracture, Fontainebleau, 1986, pp. 257-284.
- (2) Renevey, S., Thesis, Université Paris XI Orsay, France, 1997
- (3) Beremin, F.M, Met. Trans. A, Vol. 14A, 1983, pp. 2277-2287.
- (4) Mudry F., Thesis, Université de Technologie de Compiègne, 1982.
- (5) Xia, L. And Shih, C.F., J.Mech.Physic.Solids ,Vol.44, 1996, pp603-639

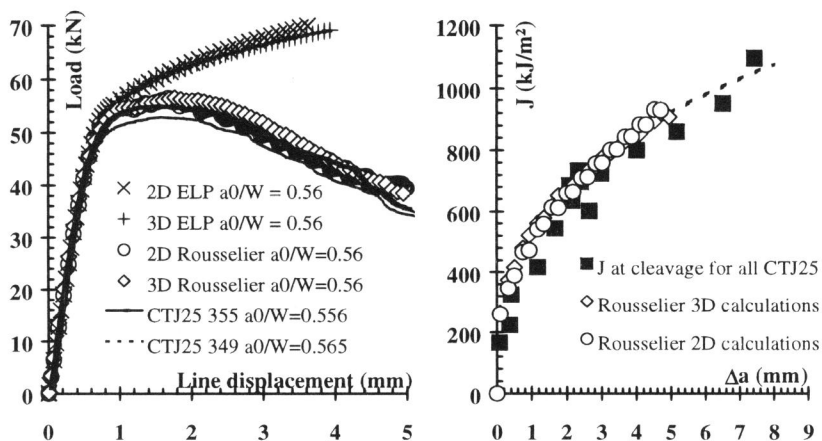


Figure 1 Comparison between computed and experimental Load opening curves

Figure 2 Comparison between computed and experimental J -  $\Delta a$  curves

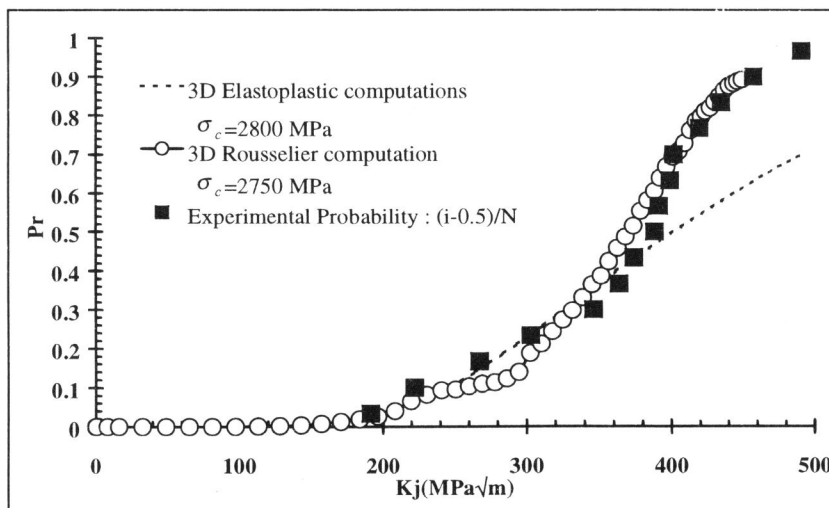


Figure 3 Comparison between computed and experimental probability to failure on CTJ25 at 0°C